FERMILAB-PUB-11-376-AD-APC

Preprint typeset in JINST style - HYPER VERSION

arXiv:1108.2235v1 [physics.acc-ph] 10 Aug 2011

Longitudinal dynamics and tomography in the Tevatron

J. Stogin[a], **T. Sen**[b] *, **R.S. Moore**[b]

[a]*Princeton University, Princeton, NJ 08544, USA*
[b]*Fermilab, PO Box 500, Batavia, IL 60510, USA*
Email: tsen@fnal.gov

ABSTRACT: Motivated by the desire to understand the longitudinal effects of beam-beam forces, we study the longitudinal dynamics of protons and anti-protons at injection and top energy in the Tevatron. Multi-turn data of the longitudinal profiles are captured to reveal information about frequencies of oscillation, and changes in the bunch distributions. Tomographic reconstruction is used to create phase space maps which are subsequently used to find the momentum distributions. Changes in these distributions for both proton and anti-proton beams are also followed through the operational cycle. We report on the details of interesting dynamics and some unexpected findings.

KEYWORDS: longitudinal dynamics; tomography; beam-beam .

*Corresponding author

Contents

1. Introduction **1**

2. Measurements of longitudinal profiles **3**

3. FFT of centroid motion **6**

4. Phase space reconstruction **10**

5. Momentum distributions **11**

6. Intensity loss **14**

7. Conclusions **16**

1. Introduction

Tomographic techniques are used to reconstruct the phase space based on one dimensional profiles measured by profile monitors. Transverse and longitudinal tomography have been used to study the development of beam tails and the onset of instabilities in several accelerators. Here we will focus on longitudinal dynamics of beams in the Tevatron as revealed by the changes in longitudinal distributions and by tomographic reconstruction using data from a wall current monitor.

Bunches are coalesced in the Main Injector and fed into the Tevatron at an energy of 150 GeV. First protons are injected, then electrostatic separators are turned on to place them on a helical orbit which is designed to separate them from the anti-protons that are subsequently injected onto a separate helical orbit. Anti-proton bunches are injected four bunches at a time into gaps between the three proton bunch trains. After each group of 3 anti-proton transfers, the gaps are cleared for the subsequent set of transfers by "cogging" the antiprotons - changing the antiproton RF cavity frequency to let them slip longitudinally relative to the protons. After acceleration to 980 GeV, the 36 proton and 36 anti-proton bunches are brought into head-on collisions at two high energy physics detectors CDF and D0. In addition to the head-on collisions, each bunch experiences 70 long-range interactions with bunches of the other beam around the ring. As a consequence of these beam-beam interactions, there is beam loss and emittance growth. The effects on the transverse dynamics has been well studied and documented [1, 2, 3]. Here we will

Parameter	Value
Top energy [GeV]	980
Number of bunches per beam	36
Proton bunch intensity	2.9×10^{11}
Anti-proton bunch intensity	0.9×10^{11}
Proton transverse normalized 95 % emittance [mm-mrad]	18
Anti-proton transverse normalized 95 % emittance [mm-mrad]	8
β^* at IP [m]	0.28
Proton rms bunch length at 980 GeV [nsec]	1.7
Anti-proton rms bunch length at 980 GeV [nsec]	1.5

Table 1. Parameters of the Tevatron

study the impact of these beam-beam interactions on the longitudinal dynamics via longitudinal tomography. The effects of the long-range interactions may be seen by comparing the longitudinal phase space and momentum distributions of protons before and after the anti-protons are injected. Effects of the head-on collisions may be found by investigating the phase space and momentum distributions of both protons and anti-protons before and after collisions are initiated. Table 1 shows some of the main parameters of the Tevatron beams.

The beam-beam force has a longitudinal component due to the coupling of the transverse motion to the electric field. This has been estimated to lead to an energy change for a test particle per interaction [4, 5] to be

$$\Delta E_{bb} = -\frac{Ne^2\alpha^*}{\beta^*} = -\frac{1}{4\pi\varepsilon_0}\frac{Ne\alpha^*}{\beta^*}\ [\mathrm{eV}] \tag{1.1}$$

where N is the bunch intensity of the opposing bunch, α^*, β^* are the Twiss parameters at the IP. Substituting values for the parameters in the Tevatron, $N_p = 2.9\times10^{11}$,$N_{\bar{p}} = 0.9\times10^{11}$, $\beta^* = 0.28$m, we have

$$\mathrm{Anti-protons:}\ \Delta E_{bb} = -1.5\alpha^*[\mathrm{keV}], \quad \mathrm{Protons:}\ \Delta E_{bb} = -0.5\alpha^*[\mathrm{keV}]$$

α^* can be in the range $\pm(0.1-1)$, so the energy change per particle per kick is of the order of keV. The relative energy change at 980 GeV is of the order of 10^{-6} per kick, this is small when compared to the energy spread in the beam, around 10^{-4}. This is a very simple estimate and there are other sources of energy change from beam-beam interactions including beams crossing at an angle and the 70 long-range interactions. It is possible that these effects are cumulative and may have an observable effect on the bunch properties. In this paper we will test this hypothesis by observing the longitudinal dynamics subsequent to the beam-beam interactions.

2. Measurements of longitudinal profiles

The longitudinal beam profiles are obtained via a resistive wall monitor in the Tevatron. This device consists of a short ceramic vacuum pipe with eighty 120 Ω resistors across it. A copper casing enclosing the ceramic break is filled with ferrite to provide a low impedance bypass for DC currents while forcing AC currents to flow through the resistors. These signals are summed into a single intensity signal which is input to a LeCroy DL7200 digital oscilloscope for data acquisition. The longitudinal beam profile was sampled at a rate of 1 GHz with periodic triggers synchronized to the RF system provided by custom electronics. These triggers were set to integer multiples of "turns" (beam revolutions) where 1 turn $\approx 21\mu$s in the Tevatron. The depth of the oscilloscope's internal data buffer limited the number of recorded triggers and the length of each digitized waveform. For our data samples, we recorded either 128 triggers of 10 μs duration (enough for 12 bunches of both beams) or 1024 triggers of 1 μs duration (enough for 5 bunches total). The digitized waveform data was read from the oscilloscope in ASCII format via an ethernet interface.

Data was taken on two days: store 7949 on July 14 2010 and store 8146 on October 6, 2010. The data was captured at different stages during injection and at top energy. The intent was to observe the effects of beam injection, acceleration and bringing the beams into collision on the longitudinal dynamics. In store 7949, data was captured at the following stages: 1) All 36 proton bunches injected and circulating on their helical orbit and four anti-proton bunches in each train injected and cogged. In the first train, anti-proton bunches A1-A4 are circulating. 2) After eight anti-proton bunches in each train (bunches A1-A8 in the first train) have been injected and cogged or moved towards the head of the proton train. 3) After all 12 anti-proton bunches in each train have been injected and cogged. This is the stage just before acceleration. 4) After acceleration to 980 GeV and final cogging and before the beta squeeze 5) After the beta squeeze and during initial collisions. 6) Beginning of data taking for high energy physics. Between stages 5 and 6, the transverse beam halo is removed using movable collimators. 7) 1 hour and 47 minutes after stage 6. At each stage, the profiles were recorded from all 12 bunches of the first train in each beam over 128 turns with some number of delays between each captured turn.

In store 8146 data was captured at the following stages: 1) Just after injecting all 36 proton bunches and opening the helix. Only protons are circulating. 2) After injecting first set of anti-protons and first cogging. There are 12 proton bunches and 4 anti-proton bunches in each train. 3) After the second set of anti-protons are injected and second cogging. 4) After the third set of anti-protons and third cogging and before acceleration. 5) After the acceleration to 980 GeV and final cogging and before beta squeeze. 6) Just after the beta squeeze and before collisions are initiated. 7) Just after initiating collisions. 8) 2 hours and 12 mins after start of collisions. At each stage the profiles were captured for 1024 turns, again with some number of delays between captured turns. The increased amount of data and the limited buffer size in the oscilloscope allowed storing data only

from the first three proton bunches P1-P3 and two anti-proton bunches A2 and A3 in the first train.

Figure 1 shows a mountain range view of the profiles of a proton bunch and an anti-proton bunch in store 7949. The profiles do not show any evidence of low frequency bunch oscillations. Earlier in Run II, such oscillations or "dancing" were observed with uncoalesced bunches[6]. Longitudinal dampers reduced the centroid oscillations at the synchrotron frequency.

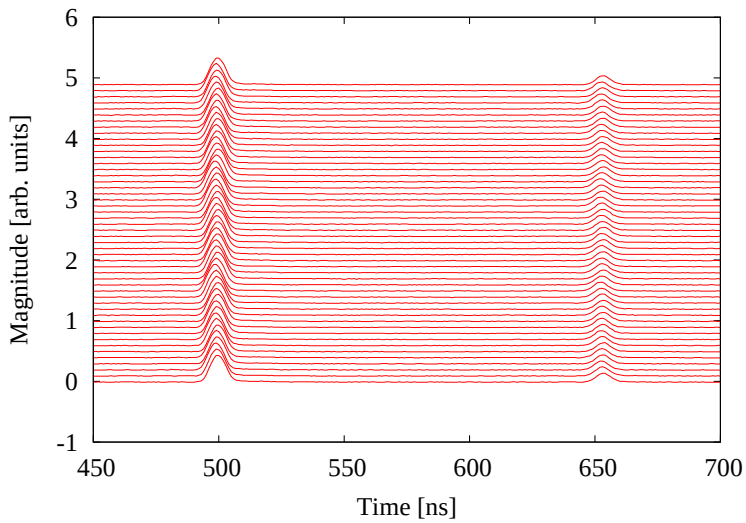

Figure 1. Part of the data from Store 7949 captured from the wall current monitor at energy 150 GeV just before acceleration. On the left is a proton bunch and on the right is an anti-proton bunch. The entire data set contains 12 proton and 12 anti-proton bunches. The initial profiles are at the bottom while the last profiles are at the top.

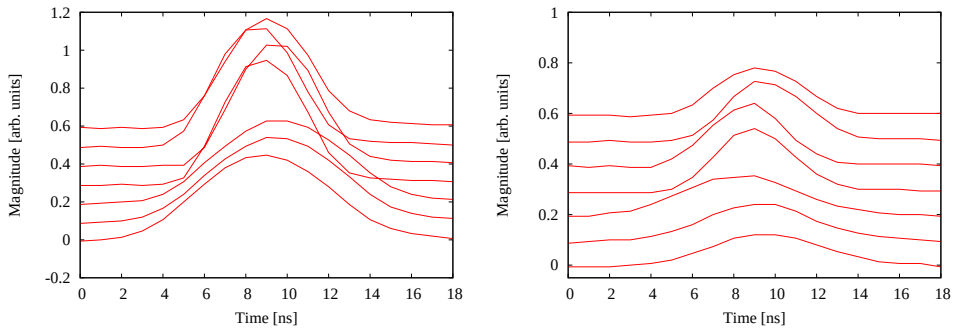

Figure 2. Store 7949: Longitudinal profile of proton bunch 1 (left) and anti- proton bunch 11 (right) at different stages from 150 GeV to 980 GeV.

Figure 2 shows the profiles of proton bunch 1 and anti-proton bunch 11 at different stages in store 7949.

The distributions can be characterized by their root mean square (rms) length and the excess kurtosis which is defined as

$$k = \frac{\sigma_4}{\sigma_2^2} - 3 \tag{2.1}$$

where σ_4 is the fourth moment and σ_2 is the second moment. The kurtosis measures the length of the tails relative to the core. This kurtosis is zero for a Gaussian, so a positive value indicates that the tails are longer than in a Gaussian distribution. Figure 3 shows

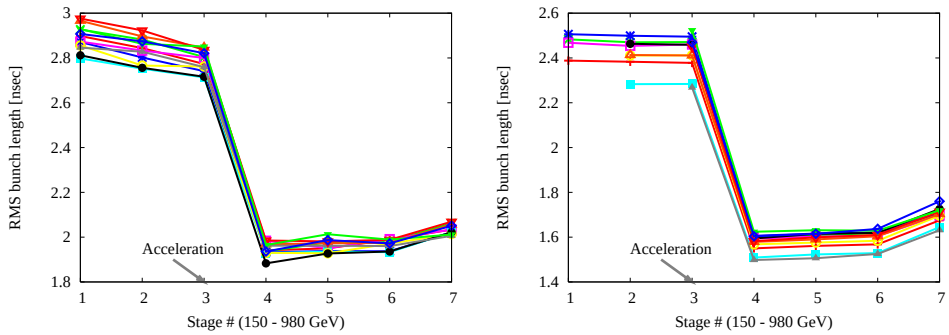

Figure 3. Evolution of the bunch length of protons (left) and anti-protons (right) for the 12 bunches during Store 7949. At the end of stage 3, beams are accelerated from 150 GeV to 980 GeV.

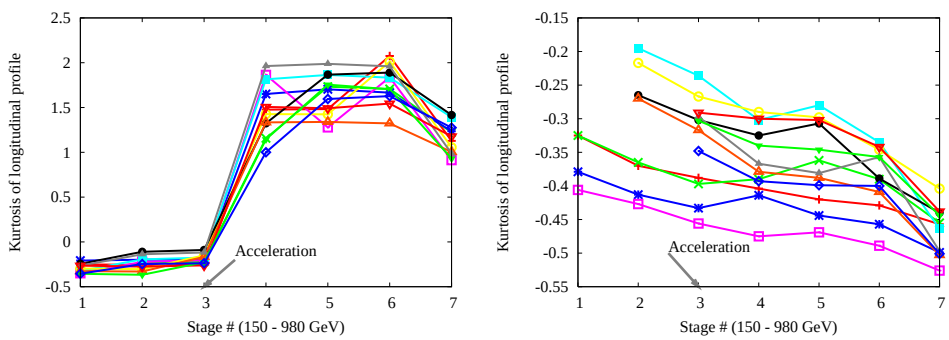

Figure 4. Evolution of the kurtosis of protons (left) and of anti-protons (right) for the bunches during Store 7949.

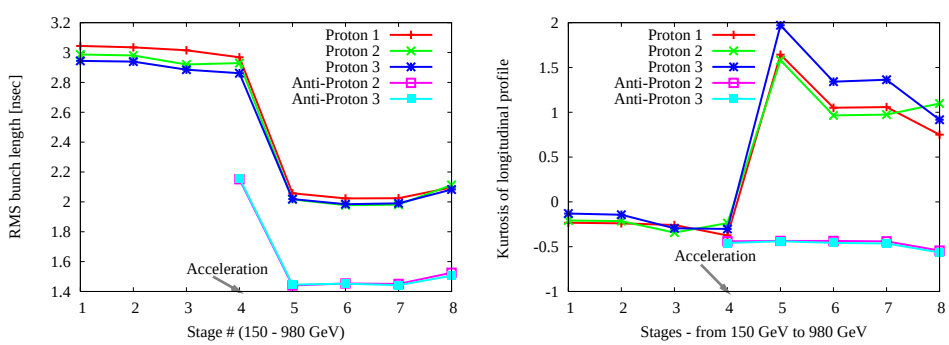

Figure 5. Evolution of the bunch length (left) and kurtosis (right) for the 5 bunches during Store 8146. In this store, acceleration occurs after stage 4.

the evolution of the bunch length of protons and anti-protons in store 7949. The proton bunches are more intense, longer and fuller in the bucket and thus more likely to be lost from the bucket. At injection energy, we see clear evidence that the bunch length of protons shrinks while the anti-proton bunch length stays nearly constant. Following the acceleration to top energy and decrease in size due to adiabatic damping, the bunch length of both species subsequently increases, primarily due to intra-beam scattering. The increase is the largest during the 2 hours between stages 6 and 7. Figure 4 shows the excess kurtosis of both species. At injection energy, the protons have negative kurtosis implying that their tails are shorter than for a Gaussian but the kurtosis gradually approaches that of a Gaussian. Following acceleration there is a rapid increase in the kurtosis even though the bunch itself is shorter, suggesting that the beam tails have grown at the expense of the core. At flat top, the kurtosis stays nearly constant for most bunches (except for a couple of bunches) until stage 6, the start of collisions, after which the kurtosis drops with time. The kurtosis of the anti-protons has a very different behaviour - they start at negative values after injection and they keep decreasing. There is no sharp rise in the kurtosis during acceleration and the decrease in kurtosis continues with time suggesting that the core is broadening at the expense of the tails.

Figure 5 shows the evolution of the rms bunch length of protons and anti-protons in store 8146. The statistical errors are smaller here since the data was averaged over 1024 samples compared to 128 samples for store 7949. Much the same conclusions on the bunch length and kurtosis apply to the behaviour in this store as well. The bunch length of protons decreases at injection energy and grows at flat top during the store for both species. Again, acceleration to top energy increases the kurtosis sharply for protons but not for the anti-protons. At flat top during the store, the kurtosis drops for both species but more quickly for protons.

During store 8130 we obtained data for the same five bunches at one stage about 12 hrs into the store. We find that the kurtosis of the 3 proton bunches had dropped to a range between 0.1 - 0.2 while the kurtosis of the anti-protons had fallen to -0.6. The proton distributions appear to approach a Gaussian distribution over long times while the distribution of the anti-protons continues to become more non-Gaussian over time with a larger core relative to the tails.

3. FFT of centroid motion

The longitudinal profiles will be used for reconstruction of the phase space as well to analyze the motion of the centroid. Good resolution of the phase space structure requires faster sampling for as many turns with as little delay as possible between turns, preferably turn by turn. On the other hand the frequency resolution of the FFT of the centroid motion is given by

$$\Delta f = \frac{1}{N\Delta t} = 2\frac{f_{max}}{N} \tag{3.1}$$

Store	Energy [GeV]	No. of samples	Delay between samples	Δf	f_{max}	N_{synch}
7949	150	128	6 turns	62.1 Hz	3976 Hz	1.5
	980	128	11 turns	33.9 Hz	2169 Hz	1.1
8146	150	1024	6 turns	7.8 Hz	3976 Hz	11.9
	980	1024	11 turns	4.2 Hz	2169 Hz	8.6

Table 2. FFT frequency resolution Δf, maximum frequency f_{max} and the number of synchrotron periods sampled N_{synch} in the two stores.

where N is the number of samples, Δt is the time delay between samples and $f_{max} = 1/(2\Delta t)$ is the maximum frequency that can be measured. If the number of samples is fixed, a larger delay Δt improves the frequency resolution but worsens the phase space resolution.

In Store 7949 the data was captured at a rate of 1 GHz for 128 turns. At 150 GeV, the time delay between each of the 128 samples was 6 turns while at 980 GeV, the delay between samples was 11 turns. In store 8146 data was captured at the same sampling rate but over 1024 turns with a delay between samples of 6 turns at 150 GeV and 11 turns at 980 GeV. Table 2 shows the frequency resolution and the maximum frequency that could be measured and the number of synchrotron periods sampled in the two stores.

Analysis shows that the Fourier spectrum of all 12 proton bunches is almost the same. There is a little more variation amongst the anti-proton bunches. These observations are valid at each of the seven stages. Between stages, the spectrum does change. The stage by stage evolution is shown in Figure 6. The surprising feature is the presence of a high frequency line in each spectrum. For every bunch, the dominant frequency at 150 GeV is 3322 Hz and for the first three stages at 980 GeV is 1744 Hz. Between the third and fourth stages (corresponding to an elapsed time of roughly 1 hr 47 mins) at 980 GeV, the dominant frequency drops by one resolution unit to 1710 Hz. It is also worth noting that the spike at the dominant frequency seems to widen at the start of initial collisions.

Figure 7 shows the spectra of the centroid motion of bunches from store 8146. While the number of bunches is less, we again observe the high frequency spike and that the centroid of each bunch has the same frequency content at each stage. All bunches show a downward shift in the centroid frequency after 2 hours into colliding mode.

It is interesting to compare the observed frequencies with some of the natural frequencies of a beam. The incoherent small amplitude synchrotron frequency is given by

$$f_s = f_0 \sqrt{\frac{h\eta e V_{rf}}{2\pi\beta E_0}} \tag{3.2}$$

where f_0 is the revolution frequency, h is the harmonic number, η is the slip factor, V_{rf} is the peak rf voltage, β is the kinematic factor and E_0 is the synchronous energy. At 150 GeV, the small amplitude synchrotron frequency is 92.7 Hz and at 980 GeV it is 36.5 Hz.

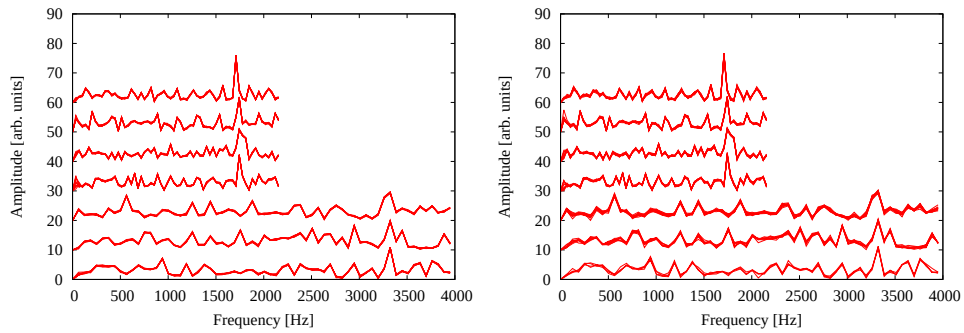

Figure 6. The Fourier spectra of all 12 proton bunches (left) and 12 anti-proton bunches (right) in store 7949 over all seven stages, starting with the first stage shown at the bottom and progressing upwards.

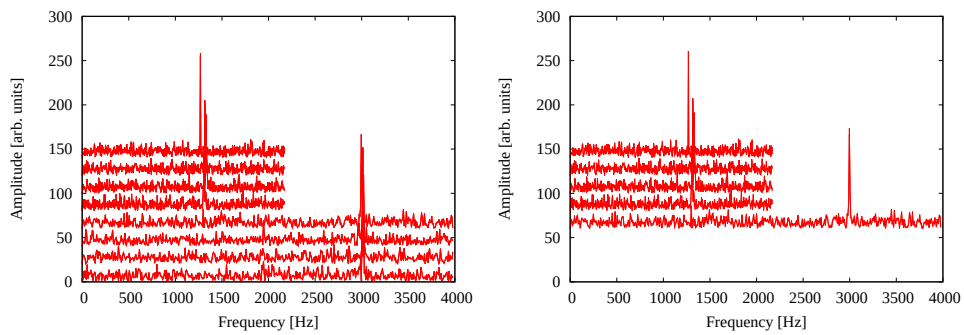

Figure 7. FFT of the centroid motion of the three proton bunches (left) and two anti-proton bunches (right) in store 8146.

More relevant is the frequency of the coherent small amplitude dipole oscillations which is the frequency when the bunch oscillates as a rigid unit. It is given by [7]

$$f_c = f_0 \left[\frac{eh|\eta|}{2\pi\beta^2 E_0} \int_{\phi_1}^{\phi_2} \lambda'(\phi)[V(\phi) - V(\phi_s)] d\tau \right]^{1/2} \tag{3.3}$$

for a bunch with a longitudinal density distribution $\lambda(\phi)$, normalized to unity $\int \lambda(\phi) d\phi = 1$, $V(\phi)$ is the rf voltage as a function of phase and ϕ_1, ϕ_2 are the endpoints of the bunch. For a Gaussian bunch and for Tevatron parameters, this frequency at 980 GeV is 32.7 Hz which is close to the incoherent frequency of 36.5 Hz.

Table 3 shows the dominant frequency observed from the FFTs of the bunch centroid motion in the two stores and the ratio of these frequencies to the coherent frequency. The existence of this high frequency line is quite unexpected and the source of these frequencies is not clear. Since the observed high frequency drops with increased energy, it suggests that it is associated with synchrotron motion. We expect that the frequency should scale as $\propto 1/\sqrt{E}$. Using this scaling, a frequency of 3322 Hz observed in the first two stages at 150 GeV in store 7949 should scale to 1300 Hz at 980 GeV. This is lower than the frequencies observed during the four stages at 980 GeV in store 7949. Similarly scaling 2996 Hz results in a frequency of 1172 Hz, also lower than the observed value in store 8146.

Store	Energy [GeV]	Stage	Frequency [Hz]	Frequency/f_c
7949	150	1	3322	101.7
	150	2	3322	101.7
	150	3	3322	101.7
	980	4	1744	53.4
	980	5	1744	53.4
	980	6	1744	53.4
	980	7	1710	52.4
8146	150	1	3020	92.5
	150	2	3020	92.5
	150	3	3012	92.5
	150	4	2996	91.7
	980	5	1312	40.2
	980	6	1329	40.7
	980	7	1316	40.1
	980	8	1269	38.9

Table 3. Dominant frequency in the FFT spectrum observed in the three proton bunches and two anti-proton bunches. All bunches have the same frequency at each stage.

Assuming that the frequency does scale with a power of the energy, data from store 7949 imply a scaling $E^{-0.34}$ while the data from store 8146 imply a scaling $E^{-0.44}$. Given that there is greater uncertainty with the data from the first store due to the lower resolution, perhaps these scalings are not entirely inconsistent.

The changes in the dominant frequency at the same energy in a store may reflect changes in the beam distribution and hence changes in the coherent frequencies. It is possible that the same harmonic of the coherent dipole frequency is excited at each stage but the coherent dipole frequency changes with the distribution.

The amplitude of oscillation in the proton bunches increases with time at 150 GeV, stays nearly constant after acceleration and then gradually decreases at 980 GeV. The amplitude is larger in the anti-proton bunches but it shows a similar behaviour with time at 980 GeV. Figure 8 shows the evolution of the amplitude of the dominant frequency for each bunch in store 8146. The origin of these high frequencies is unknown. Since all bunches in both beams have nearly the same frequencies and these lines persist for long periods of time (e.g several hours at 980 GeV) an external source associated with the rf is probably driving both beams. The fact that these high frequencies do not resonate with any of the low harmonics of the synchrotron frequency or the coherent frequency likely explains why the bunches are not perturbed by these driving frequencies.

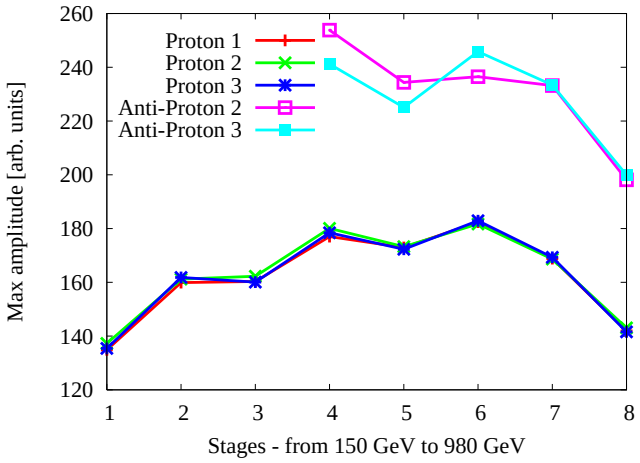

Figure 8. Amplitude of the dominant frequency in the spectrum of each bunch as it evolves during the different stages in store 8146.

4. Phase space reconstruction

We use the phase reconstruction method discussed in reference [8]. It uses a hybrid method combining algebraic reconstruction techniques (ART) and particle tracking using the difference synchrotron equations of motion. The tracking generates the coefficients in each phase space cell required during back projection from the profiles to phase space.

Representative phase space plots for store 7949 are shown in Figures 9 to 10. These show the phase space of proton bunch 1 and anti-proton bunch 11 in store 7949. Figure 11 and 12 show the phase space of proton bunch 1 and anti-proton bunch 2 during different stages of store 8146. As mentioned in Section 2, anti-proton bunches numbered 1-4 are injected during the first stage of injection but at locations closer to the tail of the proton train. They are then moved towards the head of the proton train in subsequent coggings. Consequently in store 8146, we have longitudinal profiles and phase space reconstruction at only the third stage at injection energy for the profiles of anti-proton bunches A2, A3.

The phase space plots of proton bunches at 150 GeV in both stores show small blobs at the edges and these move around in bunch phase space. These blobs are formed during coalescing of seven bunches in the Main Injector to form one Tevatron bunch. The existence of these blobs shows that the bunch is not yet in equilibrium at 150 GeV. We have found these blobs to exist in all proton bunches recorded in both stores. The more intense proton bunches nearly fill the bucket at injection and we also observe beam loss and some longitudinal clipping, e.g. in Figure 5.

The anti-proton bunches in the Tevatron are formed by the coalescing of five lower intensity anti-proton bunches in the Main Injector. The data from store 8146 allowed a finer resolution of phase space due to the greater number of projection angles. Substructure or blobs are not seen in the phase space of either of the two anti-proton bunches captured in this store and there is no observable longitudinal clipping on anti-protons at 150 GeV.

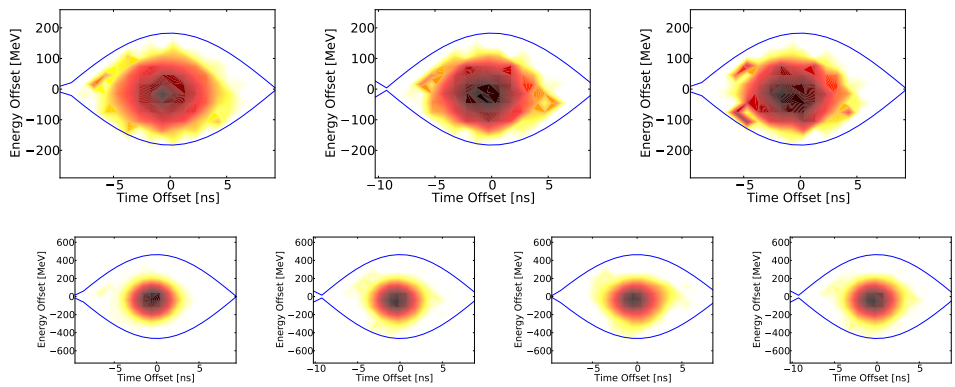

Figure 9. Proton bunch 1 in Store 7949. First three images are during injection and the last four are at top energy.

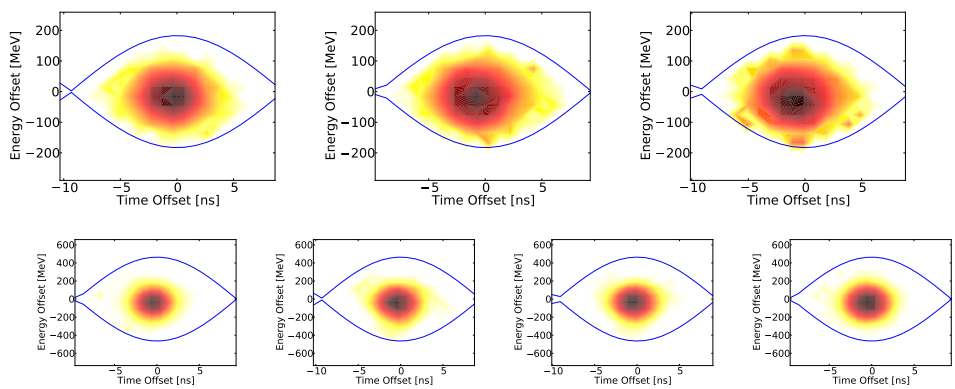

Figure 10. Anti-proton bunch 11 in Store 7949: at 150 GeV(top) and 980 GeV (bottom). The stages are the same as in Figure 9.

At 980 GeV, the bunches are smaller in the bucket and neither protons or anti-protons appear to have any structure or distortions from the expected shapes. The differences between stages are not easily discernible.

There are, of course, errors in the reconstructed phase space. Some of the errors are fundamental to the reconstruction process, others arise in the particle tracking since we assume design values for machine parameters, only the ideal rf voltage is used, and no perturbations are included in the tracking.

5. Momentum distributions

The momentum distributions can be obtained by projecting the phase space distribution onto the momentum axis. Figure 13 shows representative momentum profiles constructed for a proton bunch and an anti-proton bunch over different stages from 150 GeV to 980 GeV in store 8146. As expected, the proton bunches have a larger momentum spread at all stages.

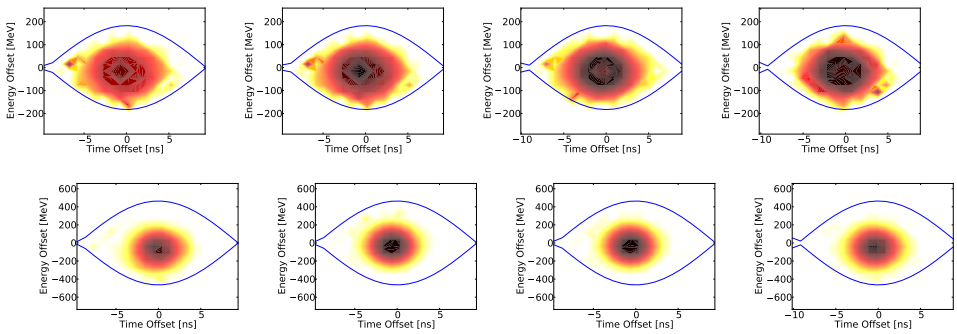

Figure 11. Phase space plots of proton bunch 1 in Store 8146 at 4 stages during injection (top) and 4 stages at 980 Gev (bottom).

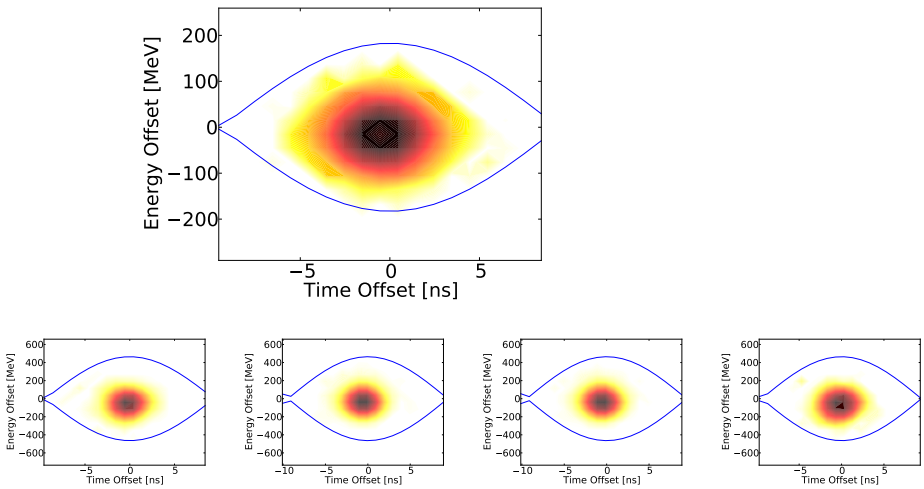

Figure 12. Phase space plots of anti-proton bunch 2 in Store 8146 at the 4th stage of injection (top) and at 4 stages at 980 Gev (bottom).

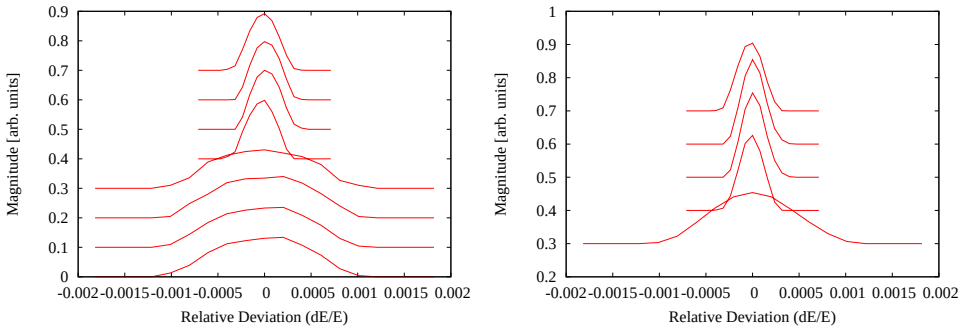

Figure 13. Momentum profiles of the first proton bunch (left) and the first anti-proton bunch (right) during the different stages from injection to 3 hours after start of collisions in Store 8146. The bottom four stages for the proton bunch and the bottom stage for the anti-proton bunch are at injection energy.

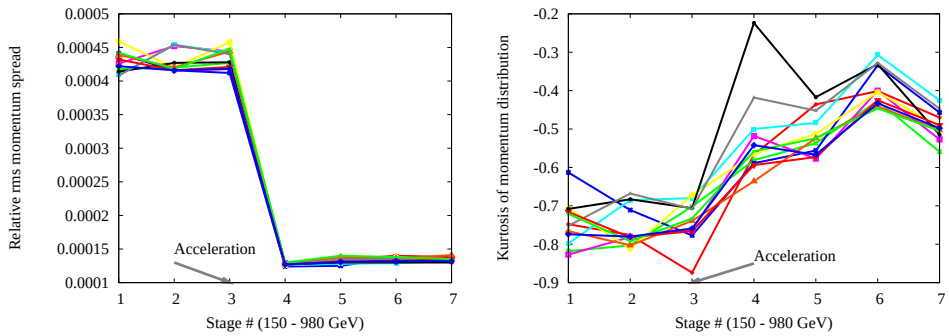

Figure 14. Evolution of the proton rms momentum spread (left) and the kurtosis of the proton momentum distribution (right) in store 7949.

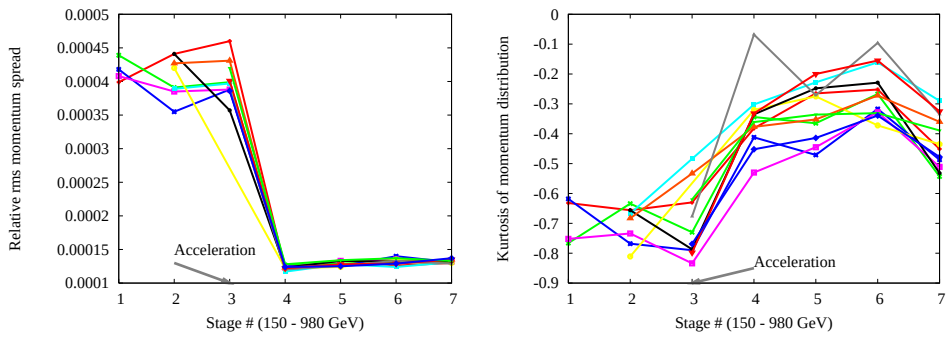

Figure 15. Evolution of the anti-proton rms momentum spread (left) and the kurtosis of the anti-proton momentum distribution (right) in store 7949.

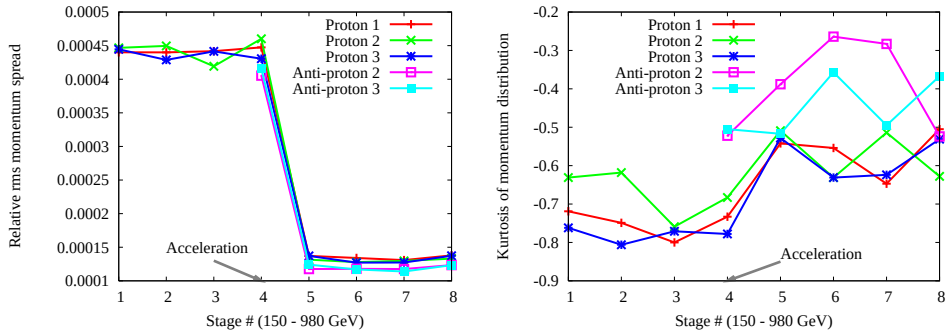

Figure 16. Evolution of the rms momentum spread (left) and kurtosis (right) during the different stages for all 5 bunches monitored in store 8146.

Figures 14 and 15 show the evolution of the rms momentum spread and the kurtosis of twelve proton and twelve anti-proton bunches in store 7949. Since we obtain a single momentum distribution for each bunch from the phase space, the errors in the calculation of these moments are larger than those in the calculations of moments of the longitudinal profiles. The sharp changes in momentum spread seen at injection energy for both beams are likely a consequence of the reconstruction errors and not physical. The large drop in the rms spread occurs as the bunch shrinks when the bunches are accelerated to 980 GeV. At top energy, the momentum spread increases gradually for all bunches and both beams. The

kurtosis of protons is negative at injection and keeps decreasing suggesting shorter tails than for a Gaussian. Acceleration increases the proton momentum kurtosis as it does for the proton longitudinal kurtosis. In general, the kurtosis increases for most bunches until collisions begin but during the store it decreases, implying that the momentum distribution does not approach a Gaussian at long times. The kurtosis of the anti-protons has a similar behaviour. We note however that the error in these kurtosis calculations which involve the fourth moment are larger than in the rms momentum spread calculations.

In store 8146, the data was collected over 1024 turns so the phase space reconstruction and hence the momentum distributions are expected to be more accurate. At injection the rms spread of the proton bunches stays nearly constant or fluctuates by small amounts. After acceleration, the momentum spread does not change much during the beta squeeze or the onset of collisions but then grows between 3-8% during the 2 hours of the store. The right plot in Figure 16 shows that the momentum distribution of the protons generally develop shorter tails at injection energy as the kurtosis decreases. During acceleration from stage 4 to stage 5 the kurtosis of all bunches increases. the behaviour after reaching 980 GeV varies from bunch to bunch. For protons the kurtosis fluctuates in a range between -0.5:-0.6 even two hours into the store. The momentum distributions of the two anti-proton bunches tend towards a Gaussian distribution until stage 6 but thereafter the kurtosis drops sharply for one bunch indicating a shortening of the tails while it fluctuates for the other bunch. These bunch by bunch differences are seen in several observables such as intensity loss and emittance growth and are often related to the individual tunes of the bunches which differ due to beam-beam effects [1].

Analysis of the data at the end of store 8130 shows that the rms energy spread for the three proton bunches and two anti-proton bunches are about the same and have grown to about 325 MeV since the start of the store. This shows that the energy spread of the anti-protons has grown much more rapidly than for protons, since the protons had a larger spread at the start of the store. The excess kurtosis of these five bunches are in the range -1.3 to -1.4 showing that the momentum distribution at long times for both species has a much shorter tail compared to a Gaussian.

6. Intensity loss

In this section we will consider the beam loss at different stages in the cycle. Since the bunch intensity is proportional to the area under the longitudinal profile, relative changes in intensity can be calculated. Figure 17 shows the relative beam loss computed from changes in the area for store 7949 during the three transitions at 980 GeV. The first transition is from before the beta squeeze to after the squeeze. The second transition occurs to the start of data taking following removal of the beam halo. The third transition is to the stage about 2 hours into the store. We observe that the beta squeeze causes some loss (about 2%) of protons but negligible losses for most anti-proton bunches. The removal of beam halo seems to reduce the beam intensity by similar amounts in both beams. The

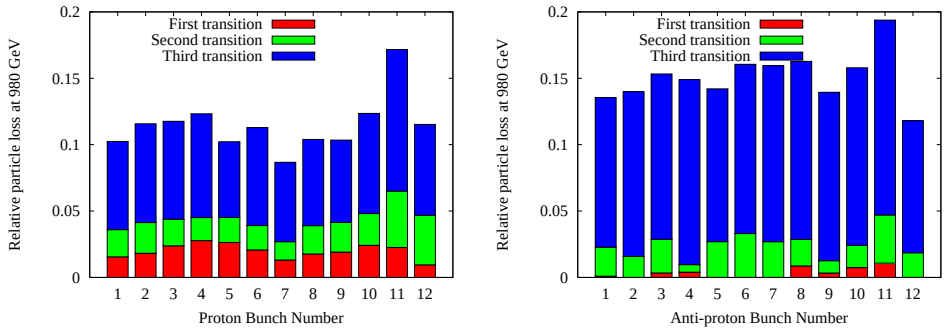

Figure 17. Relative particle loss between stages at 980 GeV for proton bunches (left) and anti-proton bunches (right) in Store 7949

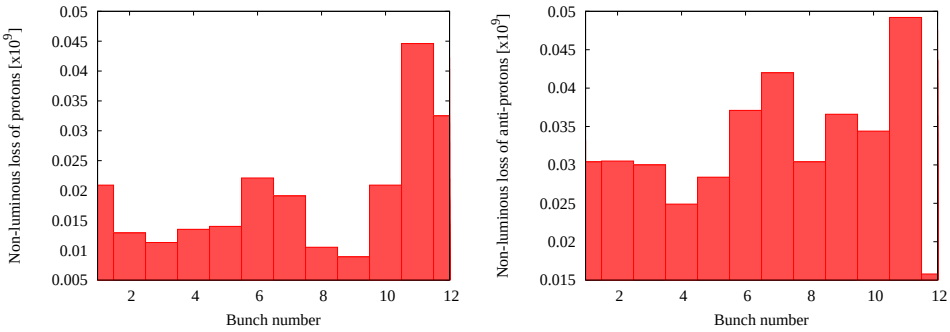

Figure 18. Bunch intensity losses not related to luminosity at the end of store 7949 for the first twelve bunches in each train. the 11th bunch in each train suffered the largest losses in accordance with the results in Figure 17 in Store 7949.

largest losses occur during the 2 hours into the store with bunch to bunch variations in both beams. It is interesting that bunches P11 and A11 have the largest losses during the store and also during the removal of beam halo. This could be due to a combination of several factors including tunes closer to the 7/12 resonance, larger emittances and intensities. The major source of beam loss is the inelastic collisions suffered by the beams at B0 and D0. The beam loss due to beam dynamics, the so-called non-luminous loss, can be obtained by subtracting the luminosity loss (determined by the instantaneous luminosity and the inelastic cross-section) from the total loss. Figure 18 shows the non-luminous loss at the end of the store for proton bunches P1-P12 and anti-proton bunches A1-A12. It is interesting that some of the bunch to bunch variation seen from the changes in bunch area are also reproduced in the non-luminous loss. Thus for example, bunches P11 and A11 suffer the largest loss in bunch area and the largest non-luminous loss. A12 has the lowest beam loss seen among the anti-protons in both figures but the relative non-luminous loss for A12 is much smaller compared to the loss from the change in bunch area.

Figure 19 shows the particle loss from the change in bunch area for store 8146. Here the first transition at 980 GeV is from before the beta squeeze to after the beta squeeze. The second transition is to a stage just before collisions are initiated. The third transition is to a stage about 2 hours after collisions started. Consistent with the data in store 7949, the beta

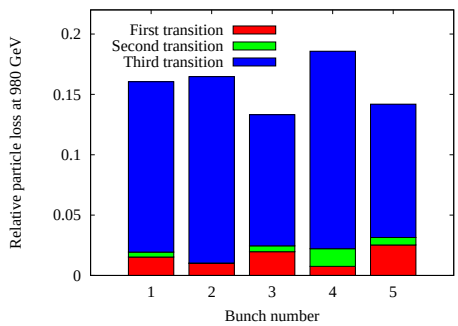

Figure 19. Relative particle loss in store 8146. Proton bunches P1-P3 are numbered 1, 3, 5 while the anti-proton bunches A2-A3 are numbered 2, 4.

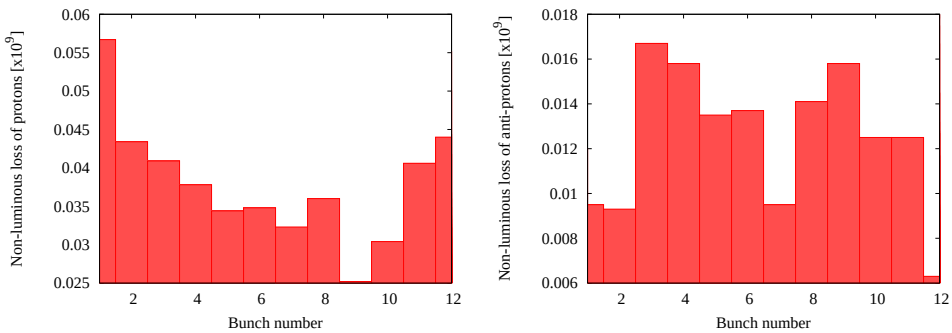

Figure 20. Bunch intensity losses not related to luminosity at the end of store 8146 for the first twelve bunches in each train. Note that the proton non-luminous losses were significantly higher than the anti-proton losses.

squeeze causes about a 2% loss in the proton bunches but much less in the anti-protons. The second transition expectedly does not cause much loss in any but one anti-proton bunch A3 for unknown reasons. Again, the dominant loss occurs during the 2 hours into the store. Comparison with the non-luminous losses in Figure 20 reproduces some of the bunch to bunch variations. For example, losses are the highest in P1 among protons and in A3 among anti-protons in both figures.

7. Conclusions

We have used the longitudinal profile of protons and anti-protons captured over many turns to study the dynamics of the beams during different stages in the Tevatron cycle. These multiple turn data sets were subsequently used for tomographic reconstructions of the longitudinal phase space which allowed us to also study the momentum distribution.

At injection energy we find that the proton bunches continue to shorten over time with some beam loss. This longitudinal clipping and beam loss is due to the larger proton emittance which nearly fills the bucket and internal motion which is also seen in the tomographic phase space reconstruction. The longitudinal beam-beam effects which should

be increasing as more anti-proton bunches are injected, likely have only a minor impact. The shape of the proton distribution, as indicated by the excess kurtosis, becomes more Gaussian during injection. After acceleration, the bunch lengths decrease but the kurtosis of the proton bunches rises sharply to a maximum value of 2 for many bunches, suggesting that the tails have increased relative to the core. After circulating for several hours during a luminosity store, the proton longitudinal distribution again approaches a Gaussian. The anti-proton bunches which have a smaller intensity and smaller longitudinal emittance behave rather differently. At injection energy, their bunch length stays nearly constant, suggesting that the long-range beam-beam effects have negligible impact. Unlike protons, their kurtosis does not increase during acceleration but instead keeps decreasing from negative values in the range (-0.25:-0.4) at injection to about -0.6 several hours into the store implying that the core keeps growing relative to the tails.

Analysis of the Fourier spectra revealed the presence of a high frequency line in both beams in both stores. This frequency which changes with energy was found to be the same for all bunches analyzed. In store 7949, this high frequency line was at 3.3 kHz at 150 GeV and it dropped to 1.7 kHz at 980 GeV while in store 8146, the line was at 3.0 kHz at 150 GeV and dropped to 1.3 kHz at 980 GeV. The amplitudes of these lines grow during injection and only start to drop a few hours after collisions start. The fact that all bunches had the same frequency and that the line persists over several hours suggests that an external source such as the rf cavity may be responsible. Since these lines are at high harmonics of the coherent synchrotron frequency, they appear to not have much impact on the beam.

The reconstructed phase space profiles show that at injection there is some substructure in the proton bunches but less so in the anti-proton bunches. Proton bunches are more intense and larger, and there may be coherent motion of smaller bunchlets within the main bunch. These bunchlets are known to be created during coalescing in the Main Injector. This motion may also be responsible for the proton beam loss observed during injection. At top energy, the phase space structure of both beams is smooth and unremarkable, at least on the resolution of our data.

The phase space distributions are used to construct a single momentum distribution for a bunch at each stage. Based on these projections, we find that the momentum distributions of both beams have shorter tails compared to Gaussian distributions and the distributions become more non-Gaussian over time. The momentum spread of the anti-protons grows at a faster rate than that of the protons. These conclusions are tentative, since the statistical error of the results obtained for the momentum distributions is significant.

Intensity losses were computed from the change in area under the longitudinal bunch profile. Stage by stage comparisons showed that the beta squeeze induces about 2% loss in protons and less so in the anti-protons. The losses during a store vary from bunch to bunch and these variations are qualitatively similar to the variations in the non-luminous losses due to beam dynamics.

We have shown that longitudinal profiles gathered over a few synchrotron periods can

be used to reveal the richness of beam dynamics and they have the potential to be equally useful in other accelerators.

Acknowledgment

This study was begun when the first author was an undergraduate intern in the Lee Teng summer internship program of 2010 at Fermilab. We thank the program for its support.

References

[1] T. Sen et al, Phys. Rev. ST-AB, **7** , 041001 (2004)

[2] V. Shiltsev et al, Phys. Rev. ST-AB, **8**, 101001 (2005)

[3] T. Sen, ICFA Beam Dynamics Newsletter, Aug 2010, pg 14

[4] V.V. Danilov et al, Proc of 1991 Part. Acc. Conf., pg 526 (1991)

[5] M. Hogan and J. Rosenzweig, Proc of 1993 Part. Acc. Conf., pg 3494 (1993)

[6] R. Moore et al, Proc of 2003 Part. Acc. Conf., pg 1751 (2003)

[7] T. Sen et al, Fermilab preprint FERMILAB-TM-2431-APC (2009)

[8] S. Hancock et al,Phys. Rev. ST-AB, **3**, 124202 (2000)